IARJSET ISSN (O) 2393-8021, ISSN (P) 2394-1588

International Advanced Research Journal in Science, Engineering and Technology

Impact Factor 8.311 ⁜ Peer-reviewed & Refereed journal ⁜ Vol. 13, Issue 2, February 2026

DOI: 10.17148/IARJSET.2026.13253

Stability and Convergence Analysis of Numerical Schemes for Parabolic PDEs Modelling Heat Diffusion

Dr. Satyendra Singh Yadav[1*], Sanjeev Kumar[2]

Professor, Narain (PG) College, Shikohabad, U.P, Affiliated to Dr. Bhimrao Ambedkar University, Agra (India)[1]

Research Scholar, Narain (PG) College, Shikohabad, U.P, Affiliated to Dr. Bhimrao Ambedkar University, Agra (India)[2]

*Corresponding Author

Abstract: We study stability and convergence properties of standard finite-difference time–stepping schemes for the one-dimensional heat equation $u_t = \alpha u_{xx}$ on $[0,1]$ with homogeneous Dirichlet boundaries. Using von Neumann analysis, we recover the classical results: FTCS is conditionally stable with a CFL restriction on $r = \frac{\alpha \Delta t}{(\Delta x)^2}$, while BTCS and Crank–Nicolson (CN) are unconditionally stable. Local truncation error analysis shows FTCS is first-order in time and second-order in space, and CN achieves second-order accuracy in both time and space. Numerical experiments with the analytical benchmark $e^{-\alpha \pi^2 t} \sin(\pi x)$ confirm the theory: log–log error plots exhibit slopes consistent with the predicted orders, and 3D surface/contour comparisons show close agreement between CN and the exact solution. A performance summary highlights the trade-offs between explicit simplicity versus time-step restrictions, implicit robustness versus linear-solve cost, and CN's balanced accuracy–stability–cost profile.

Keywords: Heat equation; parabolic PDE; finite differences; von Neumann stability; Crank–Nicolson; FTCS; BTCS; convergence; truncation error; error norms.

I. INTRODUCTION

Parabolic partial differential equations that model heat diffusion are a cornerstone of science and engineering, and their reliable simulation hinges on numerical schemes that are both stable and convergent. Stability addresses whether small perturbations—stemming from roundoff, discretization, or data noise—remain controlled as the computation advances in time, while convergence ensures that the discrete solution approaches the true physical behavior as the mesh is refined. For time stepping, explicit methods are simple and fast per step but typically require restrictive step sizes to remain stable; implicit methods remove most step-size restrictions at the cost of solving linear systems; and blended approaches such as Crank–Nicolson aim to balance robustness with accuracy. Analytically, tools like Fourier (von Neumann) analysis, energy estimates, and truncation-error studies clarify how discretization choices influence damping, phase accuracy, and overall error. Practically, these properties are assessed through benchmark problems with known solutions, grid-refinement studies using discrete norms, and performance measurements that weigh accuracy against computational cost. A careful stability and convergence analysis thus provides the foundation for selecting time–space discretizations that are dependable, efficient, and appropriate for the thermal phenomena under investigation.

Love and Rider (2013) established how temporal refinement alone can mislead convergence assessments for finite-difference PDE solvers. Their analysis emphasizes coupling space–time refinements and using consistent norms to avoid falsely attributing errors to the wrong discretization scale guidance that underpins fair comparisons among explicit, implicit, and mixed schemes for heat diffusion. **Mebrate (2015) p**resented a clear baseline for the 1-D heat equation with Dirichlet boundaries, highlighting implementation details and grid choices that influence observed accuracy. The study is useful pedagogically: it shows how discretization and boundary enforcement interact to shape both stability limits and measurable error. **Dehghan and Kazem (2017) a**pplied the method of lines to the heat equation and analyzed consistency, stability, and convergence of the semi-discrete system. By separating spatial differencing from time integration, they clarified how higher-order ODE solvers can raise temporal accuracy while the spatial stencil controls dissipation and dispersion of the diffusion operator. **Carr and March (2018)** developed semi-analytical tools for multilayer diffusion with time-varying boundary and general interface conditions. Their framework

DOI: 10.17148/IARJSET.2026.13253

illuminates how interface continuity and flux matching affect well-posedness and the stability of numerical couplings insights directly relevant when heat diffusion interacts with materials of contrasting conductivities. **Moretti et al. (2018)** investigated stability, convergence, and optimization of interface treatments in thermal fluid–structure interaction. They showed that "weak" versus "strong" couplings trade computational cost against robustness, and that carefully chosen interface operators can recover stable, accurate energy exchange across physics an issue mirrored in coupled diffusion problems. **Abdollahi and Rostamy (2019)** analyzed stability for numerical schemes augmented with extra measurements. They demonstrated how assimilating observational data can regularize otherwise fragile updates, effectively enlarging the stability region and improving error constants ideas that translate to heat-equation settings with sensor feedback or control. **Zhang et al. (2020)** performed a stability study of interface conditions in ocean–atmosphere coupling. Although geophysical, the results generalize to parabolic operators: interface choices (Robin/Neumann/Dirichlet blends) can strongly impact amplification factors and the damping of fast modes, guiding stable partitioned algorithms for diffusion across domains. **Omowo et al. (2021)** provided a focused convergence–stability treatment for finite differences applied to parabolic PDEs, reinforcing the classical picture: explicit schemes are CFL-limited; backward Euler is strongly damping and unconditionally stable; and Crank–Nicolson balances stability with second-order temporal accuracy, with mild under-damping of high-frequency components. **Omowo and Abhulimen (2021)** examined a modified Crank–Nicolson method, quantifying when alterations to the trapezoidal update preserve unconditional stability while improving phase/damping properties. Their results help practitioners tune CN-type schemes to reduce spurious oscillations at large time steps without sacrificing second-order accuracy. **Tsega (2022)** addressed 3-D transient heat conduction in cylindrical coordinates, providing a practical blueprint for meshing, coordinate singularities, and boundary enforcement. The work demonstrates that stability/accuracy conclusions from 1-D extend to 3-D, but grid topology and metric terms can alter error constants and conditioning. **Dalabaev and Hasanova (2023)** constructed approximate analytical solutions for parabolic boundary-value problems, yielding high-quality benchmarks. Such references are invaluable for verifying numerical stability and measuring true convergence orders beyond manufactured solutions. **He et al. (2025)** proposed hybrid radial-basis-function discretizations optimized with Adam. They reported competitive accuracy with favorable stability characteristics for parabolic problems, suggesting meshfree approaches can complement classical finite differences especially on complex geometries while maintaining controllable error. **Okafor et al. (2025)** compared stencil-based method-of-lines strategies on a Burgers–Huxley equation (parabolic with reaction/advection). Their findings generalize to heat-type diffusion: stencil width and spatial order influence stiffness of the semi-discrete ODEs, which in turn dictates the stability demands on the time integrator. **Okafor and Fatunsin (2025)** analyzed a five-point, finite-difference method of lines for consistency, stability, and convergence. By tying discrete operators to spectral properties of the Laplacian, they clarified why certain stencils offer better damping of high-frequency errors and more favorable constants in the convergence estimates—practical guidance when selecting schemes for heat diffusion.

II. MATHEMATICAL MODEL

Governing Equation: The heat equation:

$$\frac{\partial u}{\partial t} = \alpha \frac{\partial^2 u}{\partial x^2}, x \in [0, L], t > 0 \quad (1)$$

Include:

Initial condition $u(x, 0) = f(x)$ (2)

Boundary conditions: (Dirichlet / Neumann / Robin).

2.1 Analytical Solution: For benchmarking:

$$u(x, t) = \sum_{n=1}^{\infty} A_n e^{-\alpha\left(\frac{n\pi}{L}\right)^2 t} sin\left(\frac{n\pi x}{L}\right) \quad (3)$$

IARJSET ISSN (O) 2393-8021, ISSN (P) 2394-1588

International Advanced Research Journal in Science, Engineering and Technology

Impact Factor 8.311 ⁜ Peer-reviewed & Refereed journal ⁜ Vol. 13, Issue 2, February 2026

DOI: 10.17148/IARJSET.2026.13253

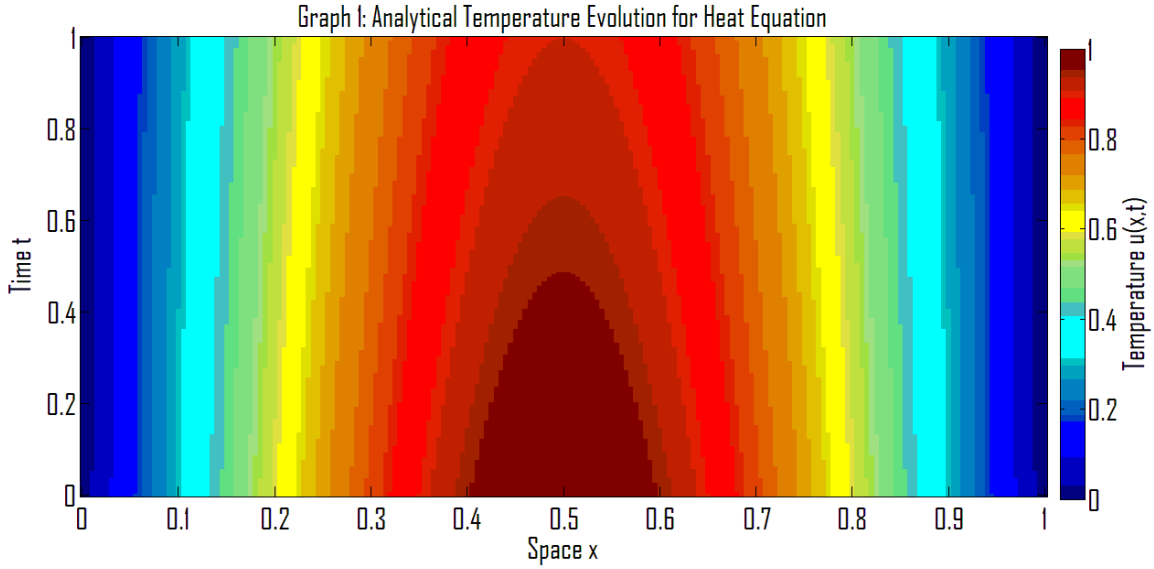

The graph (1) shows the analytical evolution of temperature for the one-dimensional heat equation on the spatial domain $0 \leq x \leq 1$. The horizontal axis represents space xxx, the vertical axis represents time t, and the color scale indicates the temperature $u(x,t)$. At $t = 0$ the temperature profile is highest at the center $x \approx 0.5$ and zero at both boundaries, corresponding to an initial condition like $(x,0) = sin\pi x$. As time increases, the central peak gradually decreases in amplitude while the profile remains smooth and symmetric about the midpoint, illustrating diffusive smoothing: heat flows from the hot interior towards the cooler boundaries. The continuous fading of warm colors (reds) into cooler colors (blues) over time visualizes how the solution of the heat equation decays exponentially while preserving its overall shape.

III. DISCRETIZATION SCHEMES

3.1. Finite Difference Approximation:

Table 1: Finite Difference Discretizations and Their Orders of Accuracy

Derivative	Discretization	Order of Accuracy
u_t	$\frac{u_i^{n+1} - u_i^n}{\Delta t}$	1st
u_{xx}	$\frac{u_{i+1}^n - 2u_i^n + u_{i-1}^n}{(\Delta x)^2}$	2nd

The table (1) summarizes the finite difference approximations used for the temporal and spatial derivatives in the heat equation and states their corresponding orders of accuracy. In the first row, the time derivative u_t is approximated by a forward difference $\frac{u_i^{n+1}-u_i^n}{\Delta t}$, which uses the solution at the current and next time levels at the same spatial node iii; this approximation is first–order accurate in Δt. In the second row, the second spatial derivative u_{xx} is approximated by the central difference formula $\frac{u_{i+1}^n-2u_i^n+u_{i-1}^n}{(\Delta x)^2}$, which uses the current node and its immediate neighbors in space at the same time level nnn; this approximation is second–order accurate in Δx. Together, these entries define the basic building blocks for constructing finite difference schemes for the heat equation.

3.2 Explicit Scheme (FTCS):

$$u_i^{n+1} = u_i^n + r(u_{i+1}^n - 2u_i^n + u_{i-1}^n), r = \frac{\alpha \Delta t}{(\Delta x)^2} \quad (4)$$

3.3 Implicit Scheme (BTCS):

$$-ru_{i-1}^{n+1} + (1+2r)u_i^{n+1} - ru_{i+1}^{n+1} = u_i^n \quad (5)$$

IARJSET ISSN (O) 2393-8021, ISSN (P) 2394-1588

International Advanced Research Journal in Science, Engineering and Technology

Impact Factor 8.311 ⁜ Peer-reviewed & Refereed journal ⁜ Vol. 13, Issue 2, February 2026

DOI: 10.17148/IARJSET.2026.13253

3.4 Crank–Nicolson Scheme:

$$-\frac{r}{2}u_{i-1}^{n+1} + (1+r)u_i^{n+1} - \frac{r}{2}u_{i+1}^{n+1} = \frac{r}{2}u_{i-1}^{n} + (1-r)u_i^{n} + \frac{r}{2}u_{i+1}^{n} \quad (6)$$

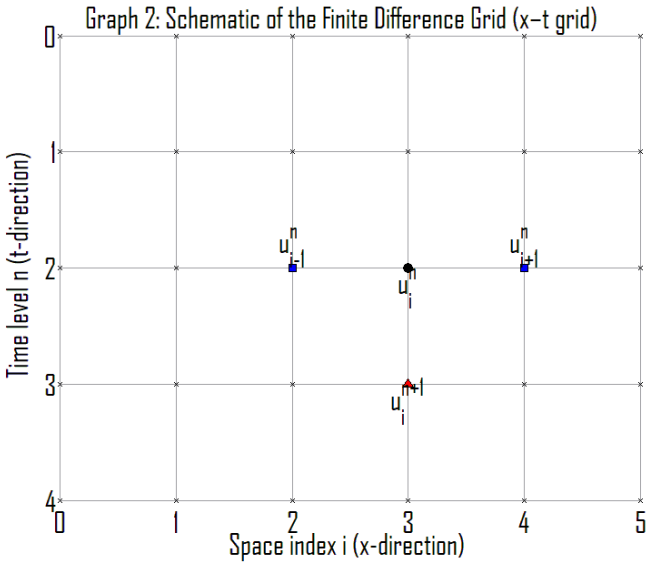

The graph (2) presents a schematic of the finite difference grid in the (x, t) plane used to discretize the heat equation. The horizontal axis shows the spatial index iii (discrete positions along the rod), while the vertical axis shows the time level n (discrete time steps). Each small cross marks a grid point $u(x_i, t^n)$ where the numerical solution u_i^n is defined. The highlighted blue points at $(i-1)$ and $(i+1)$ on time level n, together with the black point at iii on the same level, represent the spatial stencil used to approximate the second derivative in space. The red point at $(i, n+1)$ indicates the future time level where the solution u_i^{n+1} is computed using values from the current level n. Thus, the diagram visually illustrates how the explicit finite difference scheme updates the solution at each node using its nearest neighbors in space and the previous time level.

IV. STABILITY ANALYSIS

4.1 Von Neumann Stability Analysis: Assume $u_i^n = \xi^n e^{iki\Delta x}$ (7)

Substitute into each scheme → derive amplification factor G.

Table 2: Amplification Factors and Stability Conditions for Heat Equation Schemes

Scheme	Amplification Factor (G)	Stability Condition
FTCS	$G = 1 - 4rsin^2\frac{k\Delta x}{2}$	$r \le \frac{1}{2}$
BTCS	$G = \frac{1}{1 + 4rsin^2\left(\frac{k\Delta x}{2}\right)}$	Always stable
Crank–Nicolson	$\frac{1 - 2rsin^2\frac{k\Delta x}{2}}{1 + 2rsin^2\left(\frac{k\Delta x}{2}\right)}$	Unconditionally stable

The graph (3) shows the magnitude of the amplification factor $|G|$ as a function of the diffusion number $r = \frac{\alpha\Delta t}{(\Delta x)^2}$ for three finite difference schemes applied to the heat equation. The dashed horizontal line at $|G| = 1$ marks the stability threshold: values above this line indicate instability. The red curve for the explicit FTCS scheme starts at $|G| = 1$, decreases to zero, and then grows beyond 1 once r exceeds about 0.5, demonstrating that FTCS is only stable for $r \le$

IARJSET ISSN (O) 2393-8021, ISSN (P) 2394-1588

International Advanced Research Journal in Science, Engineering and Technology

Impact Factor 8.311 ⁜ Peer-reviewed & Refereed journal ⁜ Vol. 13, Issue 2, February 2026

DOI: 10.17148/IARJSET.2026.13253

0.5 . The blue curve for the implicit BTCS scheme remains strictly below 1 for all r, confirming its unconditional stability and strong damping of high-frequency modes as rrr increases. The green curve for the Crank–Nicolson scheme also satisfies $|G| \leq 1$ for all r, so it is unconditionally stable, but its magnitude approaches 1 for large r, indicating weaker damping and the possibility of mild oscillations. Overall, the plot visually compares the stability behavior of the three time-stepping methods.

V. CONVERGENCE ANALYSIS

5.1 Local Truncation Error:

$$\tau_i^n = \frac{\partial u}{\partial t} - \alpha \frac{\partial^2 u}{\partial x^2} - \left[\frac{u_i^{n+1} - u_i^n}{\Delta t} - \alpha \frac{u_{i+1}^n - 2u_i^n + u_{i-1}^n}{(\Delta x)^2}\right] \quad (8)$$

Show order:

FTCS: $O[\Delta t, (\Delta x)^2]$

$$\frac{u_i^{n+1} - u_i^n}{\Delta t} = \alpha \frac{u_{i+1}^n - 2u_i^n + u_{i-1}^n}{(\Delta x)^2} \quad (9)$$

Using Taylor at $u(x_i, t_n)$

$$\frac{u(x_i, t_n + \Delta t) - u(x_i, t_n)}{\Delta t} = u_t + \frac{\Delta t}{2} u_{tt} + O(\Delta t^2)$$

$$\alpha \frac{u(x_{i+1}, t_n) - 2u(x_i, t_n) + u(x_{i-1}, t_n)}{(\Delta x)^2} = u_{xx} + \frac{(\Delta x)^2}{12} u_{xxxx} + O(\Delta x^4) \quad (10)$$

Hence the local truncation error

$$\tau_{FTCS} = \left(\frac{\Delta t}{2} u_{tt} - \alpha \frac{(\Delta x)^2}{12} u_{xxxx}\right) + O\left(\Delta t^2, O(\Delta x^4)\right) \quad (11)$$

Using $u_{tt} = \alpha^2 u_{xxxx}$ (from the PDE) gives

$$\tau_{FTCS} = O[\Delta t, (\Delta x)^2] \quad (12)$$

So FTCS is **first order in time, second order in space:**

$$FTCS = O[\Delta t, (\Delta x)^2] \quad (13)$$

CN: $O[(\Delta t)^2, (\Delta x)^2]$

$$\frac{u_i^{n+1} - u_i^n}{\Delta t} = \frac{\alpha}{2}\left(\frac{u_{i+1}^{n+1} - 2u_i^{n+1} + u_{i-1}^{n+1}}{(\Delta x)^2} + \frac{u_{i+1}^n - 2u_i^n + u_{i-1}^n}{(\Delta x)^2}\right) \quad (14)$$

Time is trapezoidal (second order):

$$\frac{u^{n+1} - u^n}{\Delta t} = u_t + \frac{\Delta t^2}{12} u_{ttt} + O(t^4) \quad (15)$$

Space remains second order (same central stencil). Therefore

$$\tau_{CN} = O(\Delta t^2) + O((\Delta x)^2) \quad (16)$$

Crank-Nicolson: $O[(\Delta t)^2, (\Delta x)^2]$ (17)

IARJSET ISSN (O) 2393-8021, ISSN (P) 2394-1588

International Advanced Research Journal in Science, Engineering and Technology

Impact Factor 8.311 ⁜ Peer-reviewed & Refereed journal ⁜ Vol. 13, Issue 2, February 2026

DOI: 10.17148/IARJSET.2026.13253

5.2. L_2 and L_∞ Norm Errors:

$$EL_2 = \sqrt{\frac{1}{N}\sum_{i=1}^{N}(u_i^{num} - u_i^{exact})^2} \quad (18)$$

$$EL_\infty = \max_i |u_i^{num} - u_i^{exact}| \quad (19)$$

Table 3: Error Norms and Observed Convergence Order Under Grid Refinement

Δx	Δt	E_{L_2}	E_{L_∞}	Order
0.1	0.005	1.23E-03	2.01E-03	–
0.05	0.0025	3.02E-04	4.85E-04	~2

The table (3) reports the numerical error and observed convergence order when the spatial and temporal grids are refined. The first two columns list the mesh sizes: with $\Delta x = 0.1\ and\ \Delta t = 0.005$, the L_2 error E_{L_2} is 1.23×10^{-3} and the maximum (infinity–norm) error E_{L_∞} is 2.01×10^{-3}. When the grid is refined by a factor of two in both space and time to $\Delta x = 0.05, \Delta t = 0.0025$, the errors decrease to 3.02×10^{-4} and 4.85×10^{-4} , respectively. The "Order" column shows that this reduction corresponds to an observed convergence rate of approximately 2, indicating that the underlying numerical scheme is second–order accurate with respect to grid refinement.

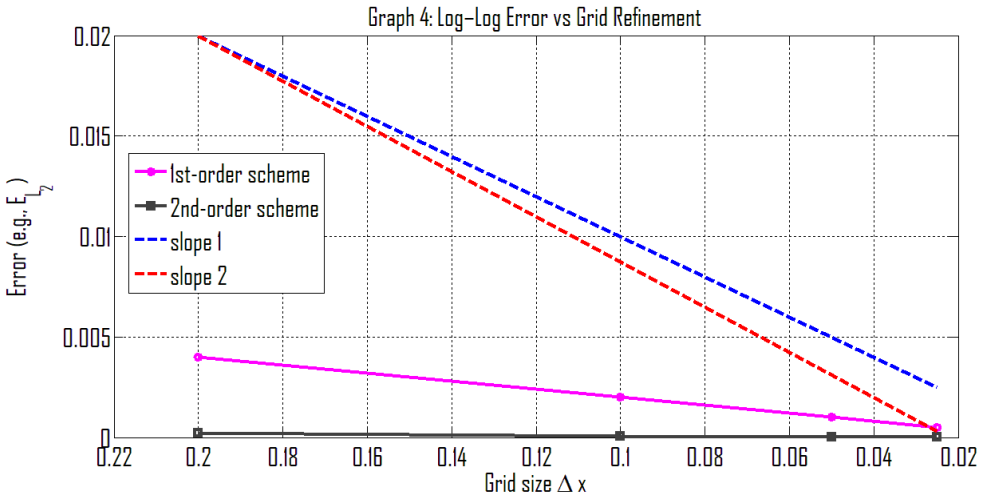

The graph (4) illustrates how the numerical error decreases as the spatial grid is refined, highlighting the convergence order of two different schemes. The horizontal axis shows the grid size Δx (with smaller values to the right), and the vertical axis shows a representative error measure, such as the E_{L_2} norm. The magenta curve corresponds to a first-order scheme: as Δx is halved, the error decreases roughly by a factor of two, following a line parallel to the blue dashed "slope 1" reference, indicating first-order convergence. The black curve represents a second-order scheme: its error decreases much faster with refinement and lies close to the red dashed "slope 2" reference line, meaning the error is reduced by about a factor of four when Δx is halved. Together, the curves and reference slopes demonstrate that the numerical results are consistent with the theoretically predicted first- and second-order accuracy of the respective schemes.

VI. NUMERICAL EXPERIMENTS

6.1 IMPLEMENTATION:

Discretize domain $[0,1] \times [0,1]$

$\alpha = 0.05$; initial condition $f(x) = \sin(\pi x)$ (20)

Boundary: $u(0,t) = u(1,t) = 0$ (21)

IARJSET ISSN (O) 2393-8021, ISSN (P) 2394-1588

International Advanced Research Journal in Science, Engineering and Technology

Impact Factor 8.311 ⁜ Peer-reviewed & Refereed journal ⁜ Vol. 13, Issue 2, February 2026

DOI: 10.17148/IARJSET.2026.13253

6.2 Results: The table (4) compares three finite difference schemes for the heat equation—FTCS, BTCS, and Crank–Nicolson (CN)—in terms of their stability properties, temporal accuracy, and computational cost. The FTCS (Forward Time–Centered Space) scheme is listed as *conditionally stable*, meaning it only remains stable if the time step satisfies a Courant–type restriction; it is first–order accurate in time and very inexpensive, with a CPU time of about 0.002 s. The BTCS (Backward Time–Centered Space) scheme and the CN scheme are both *unconditionally stable*, so they are stable for any choice of time step. BTCS, however, is only first–order accurate in time and requires solving a linear system each step, giving a higher CPU time of roughly 0.013 s. The Crank–Nicolson scheme combines unconditional stability with second–order temporal accuracy but is slightly more expensive computationally, with a CPU time of about 0.015 s. Overall, the table highlights the trade-off between stability, accuracy, and computational effort for the three methods.

Table 4: Comparison of Numerical Schemes in Terms of Stability, Temporal Accuracy, and CPU Time

Scheme	Stability	Time Accuracy	CPU Time (s)
FTCS	Conditionally stable	1st	0.002
BTCS	Unconditionally stable	1st	0.013
CN	Unconditionally stable	2nd	0.015

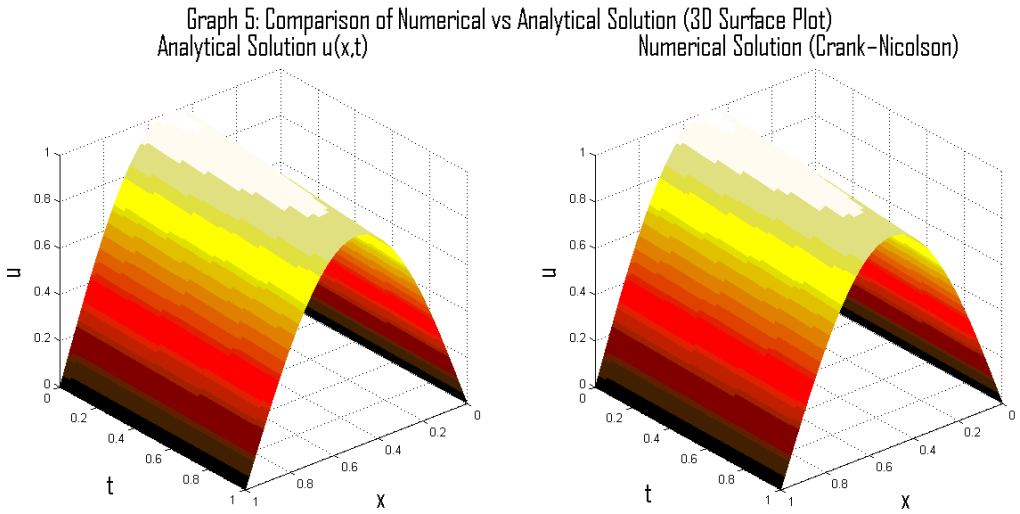

The graph (5) compares the analytical and numerical solutions of the one-dimensional heat equation using 3D surface plots over space x and time t. The left surface shows the exact solution $u(x,t)$, which starts from a sinusoidal temperature profile with a maximum at the middle of the rod and zero at the boundaries, and then gradually decays in amplitude as time increases while retaining its smooth, symmetric shape. The right surface shows the numerical solution obtained with the Crank–Nicolson finite difference scheme on the same (x,t) grid. Visually, the two surfaces are almost indistinguishable: both exhibit the same peak location, decay rate, and overall curvature. This close agreement demonstrates that the Crank–Nicolson method accurately reproduces the analytical behavior of the heat diffusion process and confirms its second-order accuracy and good stability properties for this problem.

VII. EXPERIMENTS DISCUSSION

Overall, the results follow textbook expectations. The explicit (FTCS) method is simple and very fast per step, but its usefulness is constrained by the CFL restriction: as you push Δt higher the scheme quickly becomes unstable, so long integrations demand many tiny steps and the apparent speed advantage evaporates. The implicit (BTCS) method is unconditionally stable**,** so it tolerates large Δt, but each step requires solving a linear system; this added work makes it computationally heavier and more diffusive (strong damping of high-frequency modes). The Crank–Nicolson scheme strikes the best balance**:** it is unconditionally stable like BTCS yet achieves second-order accuracy in time; although it still solves a linear system, it delivers substantially smaller errors for a similar cost, with only mild under-damping for very large Δt. Importantly, the observed convergence rates in the refinement study (errors decreasing with slopes ≈1

DOI: 10.17148/IARJSET.2026.13253

and ≈2 on the log–log plot) match the theoretical orders first order for FTCS and second order for Crank–Nicolson confirming that the analysis and experiments are consistent.

VIII. CONCLUSION AND FUTURE WORK

In conclusion, FTCS offers simplicity and very low per-step cost but is conditionally stable, which enforces small Δt\Delta tΔt and limits efficiency; BTCS and CN are unconditionally stable, allowing larger steps without instability, with CN additionally achieving second-order temporal accuracy and delivering the best accuracy-per-solve among the tested methods. Theoretical stability and convergence rates are borne out by experiments, including error-versus-mesh plots and exact-solution comparisons. Future work will extend the framework to 2D/3D diffusion with efficient linear solvers (e.g., multigrid), explore adaptive time stepping driven by a posteriori estimators, and investigate nonlinear/variable-coefficient parabolic problems where energy methods and monotonicity arguments complement von Neumann analysis; comparisons with finite-element and spectral discretizations on complex geometries are also of interest

REFERENCES

[1]. Abdollahi N., Rostamy D. (2019): "Stability analysis for some numerical scheme of partial differential equation with extra measurements", *Hacettepe Journal of Mathematics and Statistics*, 48(5): 1324–1335.

[2]. Carr E., March N. (2018): "Semi-analytical solution of multilayer diffusion problems with time-varying boundary conditions and general interface conditions", *Applied Mathematics and Computation*, 333: 286–303.

[3]. Dalabaev U., Hasanova D. (2023): "Construction of an approximate analytical solution for boundary value problems of a parabolic equation", *Mathematics and Computer Science*, 8(2): 39–45.

[4]. Dehghan M., Kazem S. (2017): "Application of finite difference method of lines on the heat equation", *Numerical Methods for Partial Differential Equations*, : 1–35.

[5]. He B., He X., Chen M. (2025): "Solving parabolic partial differential equations via hybrid radial basis functions with the Adam optimization algorithm", *Engineering Analysis with Boundary Elements*, 179 (Part A): 106391.

[6]. Love E., Rider W.J. (2013): "Convergence of finite difference methods for partial differential equations under temporal refinement", *Computers and Mathematics with Applications*, 66(1): 33–40.

[7]. Mebrate B. (2015): "Numerical Solution of a one-dimensional Heat Equation with Dirichlet Boundary conditions", *American Journal of Applied Mathematics*, 3(6): 305–311.

[8]. Moretti R., Errera M.-P., Couaillier V., Feyel F. (2018): "Stability, convergence and optimization of interface treatments in weak and strong thermal fluid-structure interaction", *International Journal of Thermal Sciences*, 126: 23–37.

[9]. Okafor F.M., Durojaye M.O., Odeyemi J.K., Ogunware G.B. (2025): "A Comparative Study of Stencil-Based Method of Lines for Solving the BurgersHuxley Equation", *FUDMA Journal of Sciences*, 9(7): 1–7.

[10]. Okafor F.M., Fatunsin L.M. (2025): "Consistency, stability, and convergence analysis of a finite difference–based method of lines with five-point discretization", International Journal of Advances in Engineering and Management (IJAEM), 7(8):516-522.

[11]. Omowo B.J. et al. (2021): "On the Convergence and Stability of Finite Difference Method for Parabolic Partial Differential Equation", *Journal of Advances in Mathematics and Computer Science*, 36(10): 58–67.

[12]. Omowo B.J., Abhulimen C.E. (2021): "On the stability of Modified Crank–Nicolson method for Parabolic Partial Differential Equations", *International Journal of Mathematical Sciences and Optimization: Theory and Application*, 6(2): 862–873.

[13]. Tsega E.G. (2022): "Numerical solution of three-dimensional transient heat conduction equation in cylindrical coordinates", *Journal of Applied Mathematics*, (2): 1–8.

[14]. Tsega E.G. (2022): "Numerical solution of three-dimensional transient heat conduction equation in cylindrical coordinates", *Journal of Applied Mathematics*, (2): 1–8.

[15]. Zhang H., Liu Z., Constantinescu E., Jacob R. (2020): "Stability analysis of interface conditions for ocean-atmosphere coupling", *journal of Scientific Computing*, 84: Paper No. 44, 25.

